Validated Spherical Pendulum Model for Rotary Liquid Slosh

Daniel D. Kana*
Southwest Research Institute, San Antonio, Texas

A combined spherical pendulum and linear pendulum system is developed to produce the same dynamic in-line and cross-axis reaction weight as liquid exhibiting rotary liquid slosh. An approximate solution of the dynamic equations for the spherical pendulum is used along with cross-axis weight measurements from slosh experiments to develop mass and damping parameters for the spherical pendulum. Similar measurements of in-line weight responses are used to develop the corresponding parameters for the linear pendulum solution. A verification of the spherical pendulum solution is accomplished by comparing the approximate solutions with those predicted by a time-step integration of the nonlinear governing equations. It is found that a constant-parameter combined system model cannot be used to represent typical rotary slosh over the entire frequency range within which this type of liquid motion response occurs. Therefore, a model is developed with some parameters constant, and others are allowed to vary as necessary to match the force data.

Nomenclature

A_o = amplitude distortion of oscillatory component θ_1
C_θ, C_ϕ = radial and circumferential damping coefficients
$F_L(\alpha)$ = amplification factor for linear pendulum response θ_2
$F_S(\alpha)$ = amplification factor for spherical pendulum response θ_1
f_n = linear natural frequency of both pendulums
g = gravity acceleration
H = liquid depth in tank
ℓ = length of both linear and spherical pendulums
m = mass of spherical pendulum corresponding to $\beta_1 W_1$ weight
t = time
W_1 = total weight of liquid
W_R, W_I = real and imaginary components of in-line weight response
W_{CC}, W_{CQ} = CO and QUAD phase components of cross-axis weight
x = excitation displacement
x_0 = amplitude of oscillatory excitation displacement
α = frequency ratio
β_1 = fraction of liquid weight W_1 represented by weight of spherical pendulum
β_2 = fraction of liquid weight W_1 represented by weight of linear pendulum
γ_0, ψ_0 = phase of oscillatory components θ_1 and θ_2, respectively
ψ = angle of nonrotating pendulum relative to excitation axis
λ_0 = combined phase angle of cross-axis weight component
ϵ_0 = phase distortion for oscillatory component θ_1
ϕ, θ = circumferential and radial coordinates for spherical pendulum
ϕ_0 = position lag angle of spherical pendulum relative to excitation plane
θ_0 = steady amplitude of spherical pendulum
θ_1, θ_2 = oscillatory amplitudes of spherical and linear pendulum, respectively
θ_A = amplitude of oscillatory component θ_1
Ω_n = circular natural frequency of oscillatory component of spherical pendulum
ω = circular frequency
ω_n = linear natural circular frequency of both pendulums
ζ_θ, ζ_ϕ = radial and circumferential damping ratios
$\zeta_{\theta 1}$ = radial damping ratio of spherical-pendulum oscillatory component at frequency 2ω
$\zeta_{\theta 2}$ = radial damping of linear-pendulum oscillatory component at frequency ω

Introduction

LARGE-AMPLITUDE slosh of liquids in moving containers manifests itself in several forms. Generally, each form has been described to some degree or another by responses of nonlinear dynamic equations that govern the motion. Much of the background for these types of propellant motions has been described in Ref. 1. Rotary liquid slosh is one form of nonlinear response that has been recognized from experiments, but because of its particular complexity, the hydrodynamic equations have never been formulated and solved. However, considerable insight into the problem has been achieved by using a support-excited spherical pendulum as a mechanical analogy of the motion. Early developments for equations of motion for this analogy are summarized in Ref. 1. However, some deficiencies were present in these early developments. More recently, Miles[2] performed a more complete analysis of the spherical pendulum that included a prediction of "deterministic chaotic" responses for some parts of the frequency range. That is, the responses were irregular in that the amplitudes and phases varied randomly with time. The existence of such responses were confirmed by Tritton[3] by means of various experiments with a spherical pendulum bob apparatus. He argues that the results can be used to study a variety of physical phenomena, including rotary liquid slosh.

During a recent study[4] of liquid slosh in scale-model Centaur rocket tanks, it was found that rotary motion was a very dominant form of response. However, this result was not anticipated, and instrumentation for measurement of cross-axis response forces were not included in that effort. Nevertheless, a compound spherical and linear pendulum model analogy was formulated[5] that successfully predicted some of the rotary slosh behavior. Both observed and predicted results

Received April 25, 1988; revision received Sept. 7, 1988.

*Institute Engineer, Department of Mechanical Sciences. Associate Fellow AIAA.

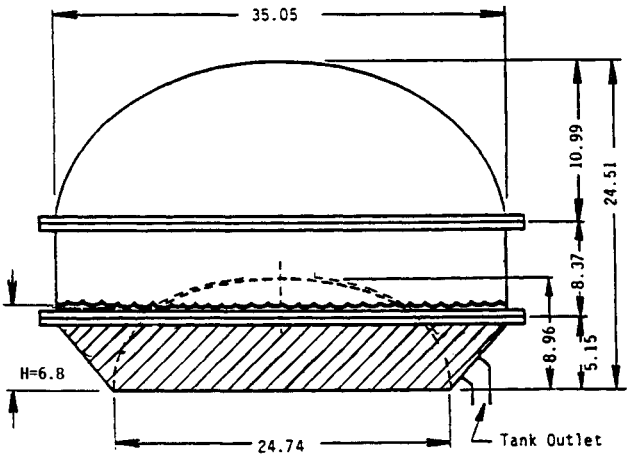

Fig. 1 Centaur G-tank (1/4.85 scale).

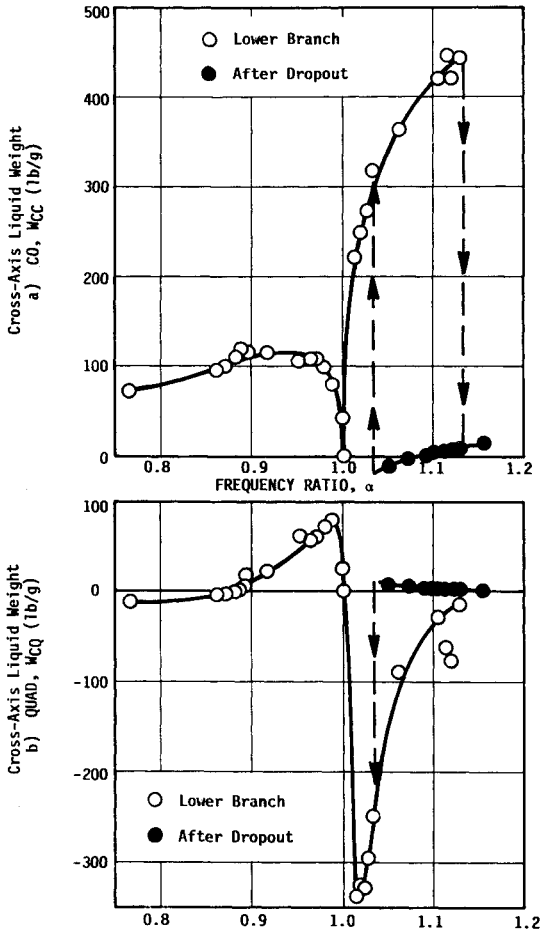

Fig. 2 Measured cross-axis weight.

did not appear to display the degree of chaotic motion described by Tritton. Therefore, a more complete experiment has been conducted for rotary slosh in the scale-model Centaur tank, and a general development of the spherical pendulum model analogy was formulated. The results of this work are presented in this paper

Experimental Study

A careful experiment was carried out with the model Centaur tank described in Fig. 1. Harmonic translation of the tank was imparted along one horizontal axis. The tank was instrumented so that liquid-weight transfer functions could be measured simultaneously in-line and cross-axis to the excitation. The liquid level shown in Fig. 1 was chosen as one that

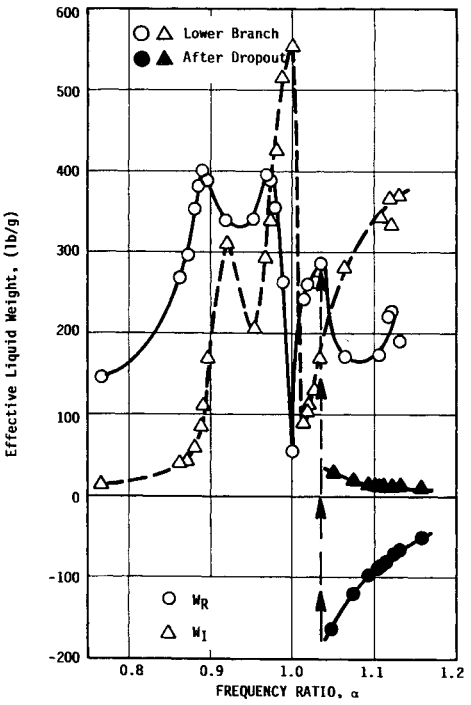

Fig. 3 Measured in-line weight.

provided optimum response measurements. (Note, this level is different from that studied in Ref. 5.) It was observed that for excitation below (but near) the linear first-mode frequency, a more-or-less planar slosh occurred. However, some cross-axis weight was present so that the planar motion apparently was tilted to the excitation axis. From this frequency to somewhat above the resonance, a very large, counterclockwise rotary response occurred at the same frequency as the excitation. The clockwise phase lag of this motion relative to the excitation axis varied from in-line to nearly 90 deg at the maximum response amplitudes, and large cross-axis weights were measured. However, for the same frequencies above resonance, a very low-amplitude, planar slosh also could occur for the same excitation conditions, and small cross-axis weights were still present. Although the rotary motion always developed counterclockwise when the frequencies were approached from below, a sustained clockwise motion of the same response amplitude could be developed by manual perturbations. The phase of this motion relative to the excitation axis varied to nearly -90 deg for the larger amplitudes. Furthermore, in the previous study,[5] it was found that the usual motions that developed were clockwise. Hence, this degree of uncertainty of the response needed to be addressed.

Reaction force and excitation-acceleration measurements were obtained for steady-state excitation of 0.2-in. peak amplitude at various frequencies that caused the rotary liquid slosh. The cross-axis and in-line forces were measured separately, and all data were digitized and subsequently reduced to weight transfer functions via fast Fourier transform techniques.[4] Figure 2 shows a plot of the cross-axis weight whose CO and QUAD parts provide phase relative to the excitation displacement. Figure 3 shows corresponding results for the in-line weight. The data indicate a quite complex type of response, although the combined system weights do display a maximum in the imaginary part W_I and nearly zero in the real part W_R at the same frequency. In accordance with similar behavior of a simple system, this frequency was designated as the linear natural frequency $f_n = 0.4470$ Hz for both pendulums of the model in Fig. 4. Thus,

$$\omega_n^2 = 4\pi^2 f_n^2 = g/\ell$$

which provides the reference for the frequency parameter α.

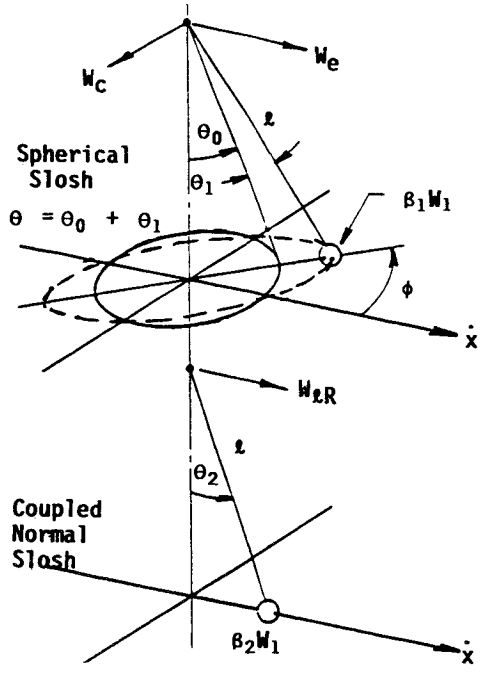

Fig. 4 Compound model for propellant slosh.

Analysis of Spherical Pendulum

Dynamical Equations

Figure 4 shows the compound spherical and linear pendulum system that was originally presented in Ref. 5. Some changes and additions of notation are necessary herein to include a description of cross-axis weights. The spherical pendulum of weight $\beta_1 W_1$ experiences responses of steady deflection amplitude θ_0, plus an oscillatory component of amplitude θ_1. The projection of the orbit onto the horizontal plane varies from an ellipse to a circle. This pendulum causes a cross-axis reaction weight of W_c and an in-line weight of W_e. The lower linear pendulum oscillates with amplitude θ_2 in the plane of excitation. It causes an in-line real weight of $W_{\ell R}$ and imaginary weight of $W_{\ell I}$ (not shown in Fig. 4). In this section, we will deal only with the dynamics of the spherical pendulum, and bring in the effects of the linear pendulum later.

The equations for the spherical pendulum were derived in Ref. 5. The general equations are

$$\ddot{\theta} + (\omega_n^2 - \cos\theta\,\dot{\phi}^2)\sin\theta + 2\omega_n\zeta_\theta\dot{\theta} + \frac{\ddot{x}}{\ell}\cos\phi\cos\theta = 0 \qquad (1a)$$

$$\sin\theta\ddot{\phi} + 2\dot{\phi}\cos\theta\,\dot{\theta} + 2\omega_n\zeta_\phi\sin\theta\,\dot{\phi} - \frac{\ddot{x}}{\ell}\sin\phi = 0 \qquad (1b)$$

wherein there has been included

$$\omega_n^2 = \frac{g}{\ell}, \quad m = \frac{\beta_1 W_1}{g}, \quad \zeta_\theta = \frac{C_\theta}{2m\omega_n}, \quad \zeta_\phi = \frac{C_\phi}{2m\omega_n} \qquad (1c)$$

These equations will be solved herein by using both a direct time-step integration approach and an approximate solution. The latter approach is necessary for a comparison with experimental weight measurements from fluid slosh experiments. Thus, it allows a determination of appropriate damping and other parameters for use in the time-step solution. Correspondence of the two approaches then provides a validation of the spherical pendulum model representation of the rotary slosh.

Reaction Weights

The reaction weight that corresponds to a reaction force F for the spherical pendulum will be defined as

$$W(\omega) = g[F(\omega)/\ddot{x}(\omega)]$$

where harmonic motion is assumed to be

$$\ddot{x} = -x_0\omega^2\cos\omega t \qquad (2)$$

The projection of the pendulum orbit onto the horizontal plane will be defined as the complex physical i-space, so that

$$\mathbf{W}_s(\omega) = W_e(\omega) - iW_c(\omega) \qquad (3)$$

where the directions for the weight components are given in Fig. 4. These two components can be evaluated as follows. The in-line weight for a *nonrotating* pendulum that oscillates in a plane at angle ψ relative to the x axis can be given as

$$W_{e\ell} = \beta_1 W_1 \ell\frac{\ddot{\theta}}{\ddot{x}}\cos\theta\cos\psi + \beta_1 W_1\frac{\ddot{x}}{\ddot{x}} \qquad (4a)$$

while the cross-axis weight for the same pendulum can be given as

$$W_{c\ell} = -\beta_1 W_1 \ell\frac{\ddot{\theta}}{\ddot{x}}\cos\theta\sin\psi \qquad (4b)$$

The effects of rotation at angular velocity ω must now be accounted for in terms of a centrifugal weight and a Coriolis weight. For the in-line weight, there results

$$W_{es} = -\beta_1 W_1 \ell\frac{\dot{\phi}^2}{\ddot{x}}\sin\theta\cos\phi - 2\omega\beta_1 W_1\ell\frac{\dot{\theta}}{\ddot{x}}\cos\theta\sin\psi \qquad (5a)$$

and for the cross-axis weight, there results

$$W_{cs} = \beta_1 W_1 \ell\frac{\dot{\phi}^2}{\ddot{x}}\sin\theta\sin\phi - 2\omega\beta_1 W_1\ell\frac{\dot{\theta}}{\ddot{x}}\cos\theta\cos\psi \qquad (5b)$$

In lieu of Eqs. (2) and (3), these may be combined to yield the following forms:

$$W_e(\omega)\cos\omega t = \frac{\beta_1 W_1\ell}{x_0\omega^2}(\dot{\phi}^2\sin\theta\cos\phi + 2\omega\dot{\theta}\cos\theta\sin\psi - \ddot{\theta}\cos\theta\cos\psi) + \beta_1 W_1\cos\omega t \qquad (6a)$$

and

$$W_c(\omega)\cos\omega t = -\frac{\beta_1 W_1\ell}{x_0\omega^2}(\dot{\phi}^2\sin\theta\sin\phi - 2\omega\dot{\theta}\cos\theta\cos\psi - \ddot{\theta}\cos\theta\sin\psi) \qquad (6b)$$

Equation (6b) will be used along with time-step solutions of Eqs. (1) to correlate with the cross-axis weight measurements from the liquid.

Approximate Solution

An approximate solution to Eqs. (1) was developed in Ref. 5. However, that solution included certain simplifying assumptions that are removed in what follows. Furthermore, a more general derivation of approximate weight expressions that correspond to Eqs. (6) also will be provided. As indicated in Fig. 4, the total deflection angle θ is composed of a steady deflection θ_0, plus an oscillatory component θ_1.

Steady Deflection

In developing an approximate solution for the steady deflection θ_0 of rotary motion at angular frequency ω, we set

$$\theta = \theta_0 \qquad (7a)$$

$$\phi = +(\omega t - \phi_0) \quad \text{CCW}, \qquad \phi = -(\omega t + \phi_0) \quad \text{CW} \qquad (7b)$$

in which either counterclockwise (CCW) or clockwise (CW)

Table 1 Possible stable solutions for rotary slosh

	Quadrant No.								
	$\alpha \leq 1$					$\alpha \geq 1$			
Equation No.	1	2	3	4		1	2	3	4
CCW									
(9b)	x[a]	x	✓[b]	✓	—	x	x	✓	✓
(8c)	✓	x	x	✓	—	✓	x	x	✓
(8d)	N/A[c]	N/A	N/A	N/A	—	x	✓	✓	x
CW									
(9c)	✓	✓	x	x	—	✓	✓	x	x
(8c)	✓	x	x	✓	—	✓	x	x	✓
(8d)	N/A	N/A	N/A	N/A	—	x	✓	✓	x

[a]No solution exists. [b]Solution exists. [c]Not applicable.

rotation is acknowledged. Thus, as indicated in Fig. 4, $+\phi$ is measured CCW relative to the excitation plane, and $+\phi_0$ is a spatial lag angle measured CW relative to that plane.

An equation that governs radial-force equilibrium is developed by substituting Eqs. (7) and (2) into Eq. (1a) and performing a harmonic balance to obtain

$$\tan\theta_0 - \alpha^2 \sin\theta_0 = \frac{\alpha^2}{2}\left(\frac{x_0}{\ell}\right)\cos\phi_0 \tag{8a}$$

in which

$$\alpha = \frac{\omega}{\omega_n} \tag{8b}$$

This expression is valid for either direction of rotation. It has solutions for

$$\text{Right-hand side} \geq 0 \qquad \text{and } \alpha \geq 0 \tag{8c}$$

$$\text{Right-hand side} \leq 0 \qquad \text{and } \alpha \geq 1.0 \tag{8d}$$

An equation that governs circumferential-force equilibrium is developed by substituting Eqs. (7) and (2) into Eq. (1b) and performing a harmonic balance to obtain

$$\zeta_\phi = +\left(\frac{\alpha x_0}{4\ell}\right)\frac{\sin\phi_0}{\sin\theta_0} \quad \text{CCW}, \qquad \zeta_\phi = -\left(\frac{\alpha x_0}{4\ell}\right)\frac{\sin\phi_0}{\sin\theta_0} \quad \text{CW} \tag{9a}$$

This expression has solutions as follows:

CCW:

$$\sin\phi_0 = +, \qquad \phi_0 \text{ is in quadrant 3 or 4} \tag{9b}$$

CW:

$$\sin\phi_0 = -, \qquad \phi_0 \text{ is in quadrant 1 or 2} \tag{9c}$$

For a steady-state rotary solution to exist for Eqs. (1), both Eqs. (8) and (9) must be satisfied in some form. A summary of the possibilities is given in Table 1. Thus, either clockwise or counterclockwise motion is predicted to exist throughout the frequency range, and for $\alpha \geq 1$, a double solution can exist for motion either way.

Oscillatory Component

It is shown by using Taylor expansion in Ref. 5 that the oscillatory component θ_1 may be approximated by an equation of the form

$$\ddot{\theta}_1 + 2\Omega_n \zeta_{\theta 1}\dot{\theta}_1 + \Omega_n^2\,\theta_1 = \frac{x_0\omega^2}{2\ell}\cos\theta_0 e^{j(2\omega t - \phi_0)} \tag{10}$$

where

$$\Omega_n = 2\omega_n, \qquad \zeta_{\theta 1} = \frac{\zeta_\theta}{2}$$

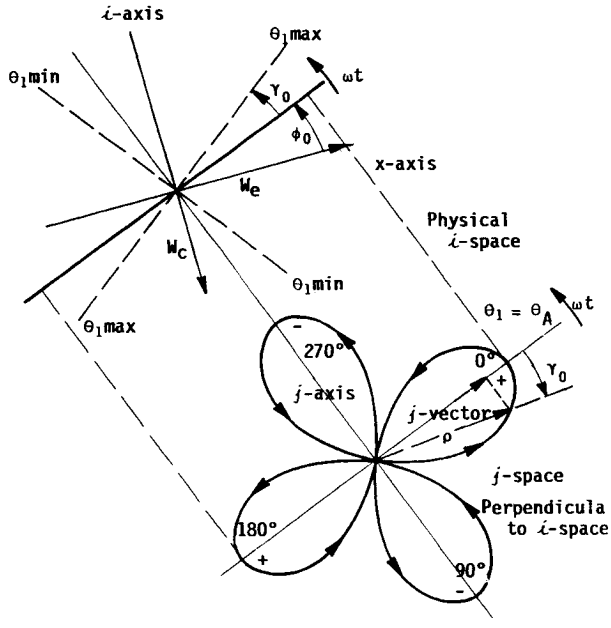

Fig. 5 Relationship of physical and complex vector spaces.

This equation represents a linear oscillator of natural frequency $2\omega_n$ and it is excited in the vicinity of that frequency. Thus, according to linear vibration theory, the response is

$$\theta_1 = \theta_A e^{-j(\gamma_0 + \phi_0)} e^{j2\omega t} \tag{11a}$$

where

$$\theta_A = \frac{x_0}{8\ell}\cos\theta_0 F_S(\alpha) \tag{11b}$$

$$F_S(\alpha) = \frac{\alpha^2}{[(1-\alpha^2)^2 + 4\zeta_{\theta 1}^2\alpha^2]^{1/2}} \tag{11c}$$

$$\tan\gamma_0 = \frac{2\zeta_{\theta 1}\alpha}{1-\alpha^2} \tag{11d}$$

$$\alpha = \frac{2\omega}{\Omega_n} = \frac{\omega}{\omega_n} \tag{11e}$$

$$\sin\gamma_0 = \frac{2\zeta_{\theta 1}\alpha}{[(1-\alpha^2)^2 + 4\zeta_{\theta 1}^2\alpha^2]^{1/2}} \tag{11f}$$

$$\cos\gamma_0 = \frac{1-\alpha^2}{[(1-\alpha^2)^2 + 4\zeta_{\theta 1}^2\alpha^2]^{1/2}} \tag{11g}$$

The complex variable j is used in the preceding expression in contrast to i, which has already been used for the horizontal physical i-plane. The complex j-plane is distinct from the i-plane, although the two are related. Furthermore, the response of θ_1 occurs at twice the circular frequency that prevails in both the i- and j-planes. Hence, further explanation of the relationship of the various complex spaces is necessary, so that the phase angles in Eq. (11a) can be interpreted properly.

One convenient representation for the relationship between the two vector spaces of concern is shown in Fig. 5. The physical i-space is shown in the horizontal plane at time $\omega t = \phi_0$. The directions on in-line weight W_e and cross-axis weight W_c are also shown. Let the complex j-space be perpendicular to the i-plane, and intersect the line at $\omega t = \phi_0$. The j-plane contains the vector that defines the oscillator response θ_1, given by Eq. (11a). In this representation,

$$\theta_1 = \theta_A e^{-i\phi_0} e^{-j\gamma_0} e^{j2\omega t} \tag{12}$$

The cloverleaf shown in Fig. 5 represents only the $\cos 2\omega t$ part of this vector. The vector ρ is traced out as its radius rotates

counterclockwise with frequency ω. The projection of the vector ρ onto the horizontal plane is approximately equal to ρ itself. By studying the diagram, it can be concluded that the interaction of the two planes is such that the projections onto the horizontal i-plane form a pair of oscillators fixed in i-space, with one in the plane at $\omega t = \phi_0 + \gamma_0$ and the other at $\omega t = \phi_0 + \gamma_0 + \pi/2$. Furthermore, the frequency of 2ω in j-space is approximately reduced to ω in these two planes. This description will be supported by the analysis that follows.

Cross-Axis Weight

The previous expressions will now be used to develop an approximate relationship for the cross-axis weight that was given by Eq. (6b). By substituting Eqs. (4) and (5) into Eq. (3), we can write the total complex weight in the i-plane as

$$\mathbf{W}_S(\omega) = -\beta_1 W_1 \ell \frac{\dot{\phi}^2}{\ddot{x}} \sin\theta e^{i\phi} + 2\omega\beta_1 W_1 \ell \frac{\dot{\theta}}{\ddot{x}} \cos\theta e^{i[\psi + (\pi/2)]}$$

$$+ \beta_1 W_1 \ell \frac{\ddot{\theta}}{\ddot{x}} \cos\theta e^{i\psi} + \beta_1 W_1 \frac{\ddot{x}}{\ddot{x}} \tag{13}$$

in which we have used

$$\psi = \omega t - (\gamma_0 + \phi_0) = \phi - \gamma_0 \tag{14a}$$

$$\sin\psi = -\cos\left(\psi + \frac{\pi}{2}\right), \qquad \cos\psi = \sin\left(\psi + \frac{\pi}{2}\right) \tag{14b}$$

In this expression, we now substitute Eq. (12) along with

$$\ddot{x} = -x_0\omega^2 \cos\omega t$$

Furthermore, we also include

$$\dot{\phi} = \omega, \qquad e^{i[\phi + (\pi/2)]} = ie^{i\phi}$$

$$\sin\theta \approx \sin\theta_0, \qquad \cos\theta \approx \cos\theta_0$$

Finally, by using sum and difference trigonometric identities, we can evaluate the product

$$e^{j2\omega t}e^{i\omega t} = \frac{1}{2}\left[(1 - ij)e^{j3\omega t} + (1 + ij)e^{j\omega t}\right]$$

$$= \frac{1}{2}\left[(1 - ij)e^{i3\omega t} + (1 + ij)e^{-i\omega t}\right]$$

where i and j denote different spaces. Note that one possible solution to this equation is $i = -j$ so that

$$e^{j2\omega t}e^{i\omega t} = e^{-i\omega t} = e^{j\omega t}$$

Note that this means that the vector in j-space rotates opposite to the direction indicated in Fig. 5. However, the phase angles in j-space can remain as defined.

With these expressions, the left-hand term in Eq. (13) contains only $\cos\omega t$, whereas after expansion, the right-hand side contains both $\cos\omega t$ and $\sin\omega t$ terms. If, as an approximation, only $\cos\omega t$ terms are collected, and we define

$$\lambda_0 = 2(\gamma_0 + \phi_0) \tag{15}$$

then Eq. (13) reduces to

$$\mathbf{W}_S(\omega) = \beta_1 W_1 \frac{\ell}{x_0}\left(\sin\theta_0 \cos\phi_0 - i \sin\theta_0 \sin\phi_0\right)$$

$$+ \beta_1 W_1 \cos^2\theta_0 F_S(\alpha)\,(\cos\lambda_0 - i \sin\lambda_0) + \beta_1 W_1 \tag{16}$$

From this we can define, along the real cross-axis, a co-phase component:

$$W_{CC} = \beta_1 W_1 \left[\frac{\ell}{x_0} \sin\theta_0 \cos\phi_0 + \cos^2\theta_0 F_S(\alpha) \sin\lambda_0\right]$$

$$= W_c(\omega) \tag{17a}$$

and, along the in-line axis, a quadrature-phase component:

$$W_{CQ} = -\beta_1 W_1 \left[\frac{\ell}{x_0} \sin\theta_0 \cos\phi_0 + \cos^2\theta_0 F_S(\alpha) \cos\lambda_0\right]$$

$$= \beta_1 W_1 - W_e(\omega) \tag{17b}$$

where W_{CQ} is taken as positive to the left.

These expressions can be evaluated by comparison with direct cross-axis weight measurements.

Combined System Reaction Weights

The total reaction weights for the combined effect of the spherical pendulum, plus the linear pendulum, can now be given as the in-line component

$$W_R = W_1 - W_{CI} + \beta_2 W_1 F_L(\alpha) \cos\psi_0 \tag{18a}$$

and imaginary (note, not the cross-axis) component

$$W_I = W_{CR} + \beta_2 W_1 F_L(\alpha) \sin\psi_0 \tag{18b}$$

so that the total vector weight measured along the in-line axis is

$$\mathbf{W}_{\ell R} = W_R - iW_I \tag{19a}$$

wherein

$$\psi_0 = \arctan\left(\frac{W_1 - W_{CR}}{W_R - W_1 + W_{CI}}\right) \tag{19b}$$

In the preceding expressions,

$$F_L(\alpha) = \frac{\alpha^2}{[(1 - \alpha^2)^2 + 4\zeta_{\theta 2}^2\alpha^2]^{1/2}} \tag{19c}$$

in which $\zeta_{\theta 2}$ is the damping for the linear oscillator and β_2 is its mass fraction. The amplitude for the linear oscillator is based on the form derived in Ref. 4. However, its phase angle is given by Eq. (19b), which is derived from Eq. (18). Hence, if any phase distortion exists because of coupling between the two oscillators, that distortion is accounted for.

System Identification Correlation

Spherical Pendulum

Approximate Solution

The previous developments are now used in conjunction with the experimental cross-axis weight data of Fig. 2 and visual observations of the rotary slosh to determine parameters for the model. It was observed that the steady amplitude of the rotary slosh became increasingly larger for increasing frequency, until at a point above $\alpha = 1.0$, where the response dropped out to essentially a planar response at very low amplitude. Furthermore, just before dropout, the phase angle ϕ_0 of CCW rotary motion was very nearly 90 deg. With this information, Eqs. (8) and (9) were programmed on a personal computer to be solved simultaneously by trial and error. The excitation x_0, pendulum length ℓ, and frequency ratio α were known inputs used along with an assumed value of circumferential damping ζ_ϕ, and an initial iteration value of the steady deflection θ_0 to compute position lag angle ϕ_0 from Eq. (9a).

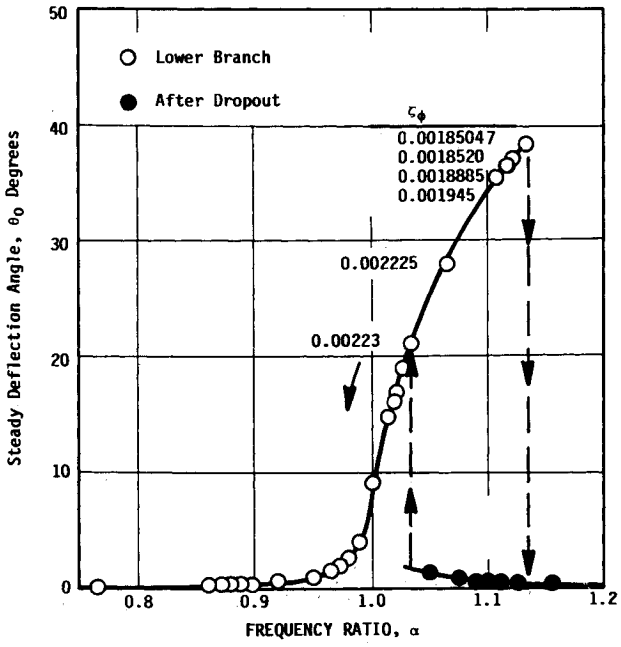

Fig. 6 Steady deflection angle.

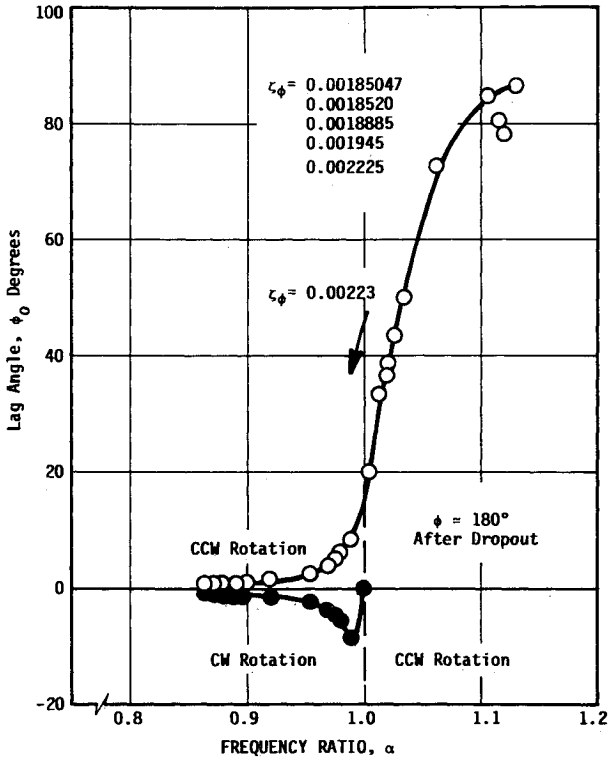

Fig. 7 Position lag angle.

The result was then input to Eq. (8) to compute each side of the expression. The process was repeated with an incremental increase or decrease on θ_0 until the two sides of Eq. (8a) were within 1%. This iteration was repeated by trial and error for values of ζ_ϕ, which ultimately resulted in $\phi_0 \simeq 90$ deg for the value of α just before the dropout response-frequency ratio of $\alpha = 1.135$. Thereafter, the entire process was repeated for each value of frequency, so that the corresponding visually observed values of position angle ϕ_0 resulted from the calculations. The observed values for ϕ_0 decreased to near zero for frequencies below $\alpha = 1.0$. By repeating this process at each frequency point at which data were acquired, the response curves of Figs. 6 and 7 resulted. In Fig. 6, it can be seen that the damping ζ_ϕ had to be increased slightly for lower frequencies, to where it could be held constant at $\zeta_\phi = 0.00223$. For frequencies below $\alpha = 1.0$, the response was so small that ϕ_0 could not be discerned visually. Hence, the rotation may have been either CW or CCW in this region, as indicated in Fig. 7. Thus, a plausible range of values for the damping ζ_ϕ was established, which resulted in computed values of steady deflection θ_0 and position angle ϕ_0 that qualitatively agreed with the visual observations on ϕ_0.

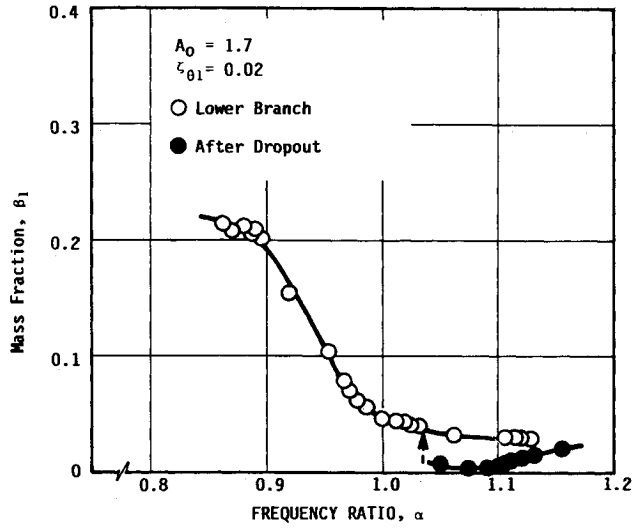

Fig. 8 Spherical pendulum mass fraction.

Next, other parameters were determined by a similar iteration of the cross-axis weights given by Eqs. (17a) and (17b). These two equations were solved for $\beta_1 W_1$ and set equal to each other to result in

$$W_{CC}\left[\frac{\ell}{x_0}\sin\theta_0\cos\phi_0 + \cos^2\theta_0 F_S(\alpha)\cos\lambda_0\right] = -W_{CQ}\left[\frac{\ell}{x_0}\sin\theta_0\sin\phi_0 + \cos^2\theta_0 F_S(\alpha)\sin\lambda_0\right]$$

in which λ_0 is given by Eq. (15) and $F_S(\alpha)$ is given by Eq. (11c). If one assumes a damping value $\zeta_{\theta 1}$, both sides of the preceding equation can be calculated by including all previously determined information for each frequency point along with

$$\gamma_0 = \arctan\left(\frac{2\zeta_{\theta 1}\alpha}{1-\alpha^2}\right)$$

Thus, by starting with an initial value of $\zeta_{\theta 1}$, the equation was iterated until the two sides were equal within 1%. Then, with the final value of $\zeta_{\theta 1}$, the mass fraction β_1 was calculated from Eq. (17a) or (17b).

With the preceding approach, it was found that plausible solutions for β_1 (i.e., $\beta_1 < 1$) still could not be obtained throughout the frequency range. By comparing with the time-step solutions (to be described later), it was found that both amplitude and phase distortions on θ_1 had to be allowed for in order for plausible values of β_1 to result. Thus, we set

$$\lambda_0 = 2(\gamma_0 + \phi_0) + \epsilon_0$$

$$\theta_A = A_0\theta_A$$

By trial and error, it was found that constant values of $A_0 = 1.7$ and $\zeta_{\theta 1} = 0.02$, along with a variable ϵ_0, provided the set of results given in Fig. 8 and 9. It was concluded that the necessity for the amplitude and phase distortions stems from the use of the approximate linear equation (10) for determining θ_1, rather than the actual nonlinear equation that governs that response, and from the fact that Eq. (16) is only an approximate expression.

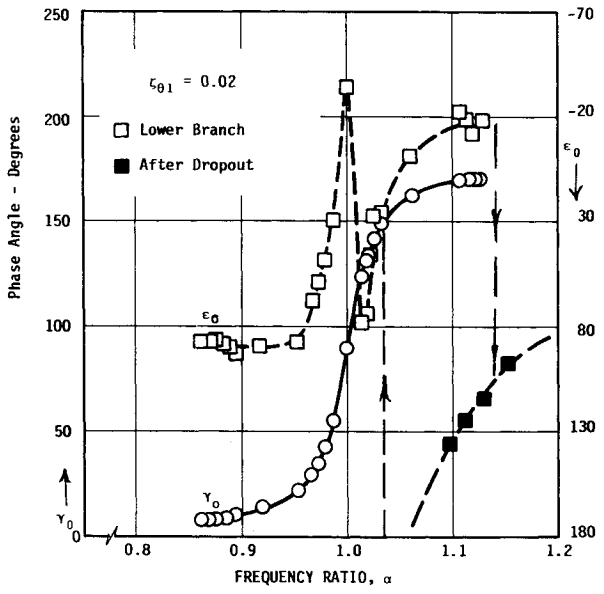

Fig. 9 Phase response.

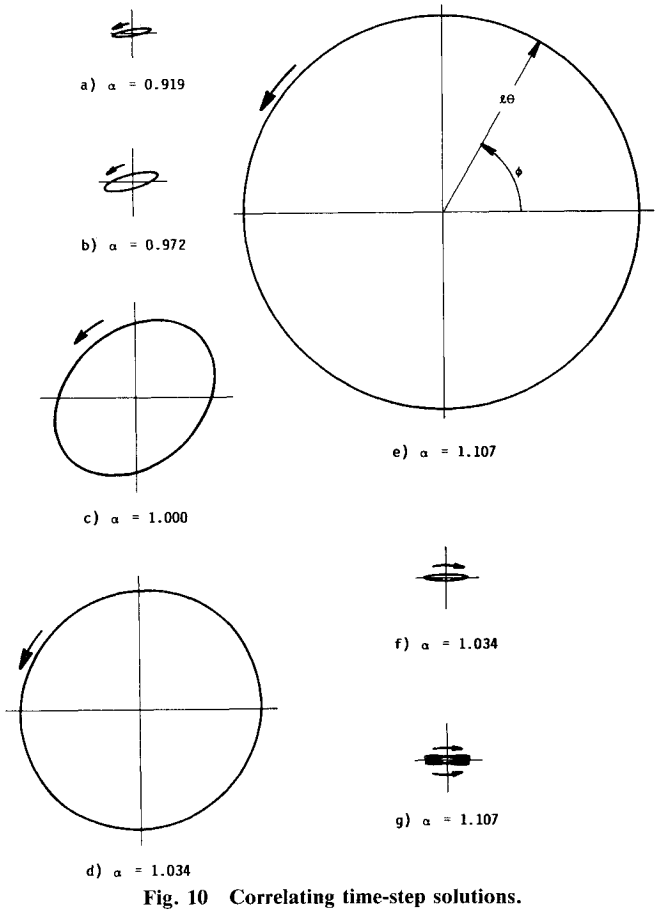

Fig. 10 Correlating time-step solutions.

With the preceding approach, Figs. 6–9 show one model representation for a spherical pendulum that produces nearly the same weight response as that of the fluid. To validate this assertion, several select values of frequency were chosen for computation of comparative data from time-step solutions of the original nonlinear equations.

Time-Step Solution

Validation of the parameters predicted by the approximate solution was accomplished by using these parameters in Eqs. (1a), (1b), and (6b) to compute the cross-axis weight and

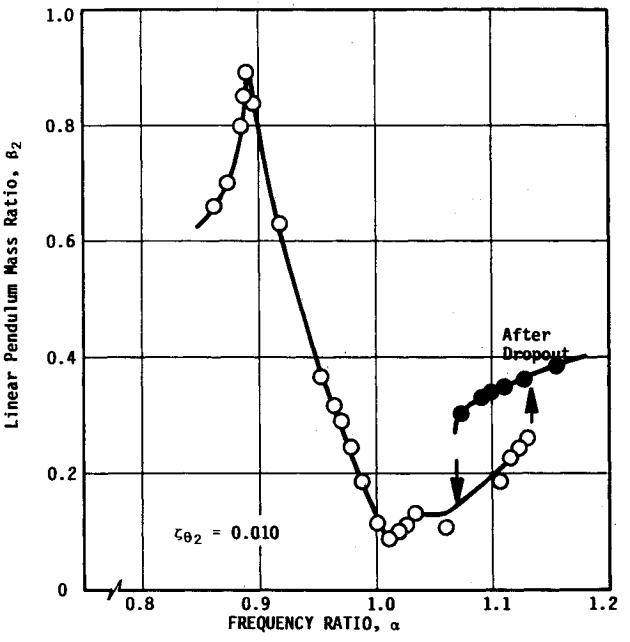

Fig. 11 Linear pendulum mass fraction.

comparing with experimental values at the select frequency points. For example, from the preceding figures at $\alpha = 0.972$, the following set of parameters were selected for a case of CCW motion:

$$\zeta_\phi = 0.00223, \quad \theta_0 = 1.965 \text{ deg}, \quad \phi_0 = 4.415 \text{ deg},$$

$$W_{CR} = 108.0 \text{ lb}, \quad W_{CI} = 59.57 \text{ lb}, \quad \zeta_{\theta 1} = 0.020,$$

$$\beta_1 = 0.0695, \quad \gamma_0 = 35.186 \text{ deg}, \quad \epsilon_0 = 58.5 \text{ deg}$$

The appropriate parameters were substituted into Eqs. (1a) and (1b) and a time-step solution performed at increments of 0.002 s by means of a program called DYSIM (Dynamic Simulation). This program integrates coupled first-order differential equations by a fourth-order Runge-Kutta integration process. Time histories for the preceding cases clearly demonstrate a steady response after the solution has stabilized. For this case, θ maintains a steady amplitude that corresponds to that given for θ_0 above, plus a double frequency oscillation of amplitude that is about 1.7 times that predicted by Eqs. (11b) and (11c) of the approximate solution. Subsequently, the time-step solution values for θ were substituted into Eq. (6b) to predict the cross-axis weight. The resulting time history for W_C contained a dominant component at frequency ω, and the amplitude of this component was about 120 lb. This very nearly corresponds to the square root of the sum of the squares of W_{CC} and W_{CQ} given by the experimental data.

A projection of the spherical pendulum response onto the horizontal plane for the preceding case is given in Fig. 10b. Similar solutions for several other frequencies and their corresponding parameters given in Figs. 6 and 7 are also shown to approximate scale in Fig. 10. It was found that these steady solutions would develop for any CCW initial angular velocity, although various unsteady motions may exist at the start of the solution, depending on the initial conditions. However, note that double solutions exist for some frequencies of $\alpha > 1$. (This agrees with Fig. 6.) The resulting solution depended on the initial conditions. Furthermore, although CCW solutions are shown for the lower-frequency large-amplitude branch, solutions after dropout were much smaller, essentially planar, and the direction of rotation was opposite for $\alpha = 1.034$, while the direction was unsteady with a periodic change at $\alpha = 1.107$.

Finally, it should be mentioned that another set of solutions for CW motion also was verified for the frequencies shown in Fig. 10, along with their corresponding parameters. For these

cases, the solutions were the mirror image about the x axis, compared to those given in Fig. 10. In all cases studied, the magnitudes of the cross-axis weights predicted by the time-step solutions compared quite well with the experimental values. The phases varied somewhat, depending on the conditions. Thus, a reasonable validation of the spherical pendulum for representing the cross-axis effect of the rotary liquid slosh was established.

Combined System

The remaining parameters for the lower linear pendulum were determined by substituting experimental weight data from the liquid into Eqs. (18) and (19). For this, a constant damping value $\zeta_{\theta 2} = 0.01$ was assumed. The resulting weight ratio β_2 for the corresponding linear pendulum is given in Fig. 11. It may be noted that, besides also displaying a significant variation with frequency (as did the parameters for the spherical pendulum), the sum of the two weight ratios $(\beta_1 + \beta_2)$ is greater than 1.0 for $\alpha \simeq 0.89$. This poses no contradiction, as the complex vector component of weight along each axis does not exceed the total weight W_1 for the liquid.

Discussion

The preceding development demonstrates that the combined spherical and linear pendulums can be used as an analog for rotary liquid slosh so that similar cross-axis and in-line weights are produced for steady-state, harmonic excitation. However, some parameters vary significantly with frequency, so that a constant-parameter analogy could be used for arbitrary time-history excitations only if prediction of the largest weight response were sufficient. Even this result is very useful for satellite propellant-dynamics applications.

It is well to reflect on the value of the approximate solution and time-step solutions as a tool for predicting the responses of the combined analytical model. In fact, the time-step solution provides the most accurate results, although given a set of experimental weight data for the fluid, it would be difficult to use this approach alone to develop model parameters. A trial-and-error process that includes significant computer time would be necessary. A more practical approach is to use the approximate solution developed herein for determining the parameters, and verify the results for select cases by means of the time-step approach.

One of the most significant results from this work is evidence that the spherical pendulum was quite well-behaved in exhibiting rather predictable steady-state solutions for the cases studied (see Fig. 10). This result appears to disagree with the general description given for observations made in Ref. 3. Here, except for the direction of rotation depending on initial conditions, a "chaotic" type of motion appears to occur only for frequencies above the dropout response. It may be that, in fact, the value of the circumferential damping ζ_ϕ is the major parameter that determines how "well-behaved" the larger-amplitude motions are. It is suspected that lower values of circumferential damping would result in more chaotic motions.

Acknowledgments

This project was conducted under the SwRI Internal Research Program, whose support is gratefully acknowledged. Furthermore, the contributions of several staff members are recognized. Mr. Steven T. Green performed the digital computations for the time-step solutions. Mr. Rick Pitman performed the experiments under the guidance of Mr. Dennis C. Scheidt. Additional assistance was provided by Mr. Victor Hernandez and Mrs. Donna Alexander. The author expresses his sincere appreciation to all these individuals.

References

[1] *The Dynamic Behavior of Liquids in Moving Containers,* edited by H. N. Abramson, 2nd Printing, Southwest Research Institute, San Antonio, TX, NASA SP-106, 1966.

[2] Miles, J. W., "Resonant Motion of a Spherical Pendulum," *Physica,* Vol. 11D, 1984, pp. 309–323.

[3] Tritton, D., "Chaos in the Swing of a Pendulum," *New Scientist,* Vol. 24, July 1986, pp. 37–40.

[4] Unruh, J. F., Kana, D. D., Dodge, F. T., and Fey, T. A., "Digital Data Analysis Techniques for Extraction of Slosh Model Parameters," *Journal of Spacecraft and Rockets,* Vol. 23, March–April 1986, pp. 171–177.

[5] Kana, D. D., "A Model for Nonlinear Rotary Slosh in Propellant Tanks," *Journal of Spacecraft and Rockets,* Vol. 24, March–April 1987, pp. 169–177.